HHS Public Access

Author manuscript

Cell. Author manuscript; available in PMC 2017 August 11.

Published in final edited form as:

Cell. 2016 August 11; 166(4): 991–1003. doi:10.1016/j.cell.2016.06.058.

Immune Monitoring Of Trans-Endothelial Transport By Kidney Resident Macrophages

Efstathios G. Stamatiades[1], **Marie-Eve Tremblay**[2,3], **Mathieu Bohm**[1,4], **Lucile Crozet**[1,5], **Kanchan Bisht**[2,3], **Daniela Kao**[6], **Carolina Coelho**[1], **Xiying Fan**[1,7], **William T. Yewdell**[1], **Anne Davidson**[8], **Peter S. Heeger**[9], **Sandra Diebold**[10], **Falk Nimmerjahn**[6], and **Frederic Geissmann**[1,4,5]

[1]Immunology Program and Ludwig Center at Memorial Sloan Kettering Cancer Center, Memorial Sloan Kettering Cancer Center, 417 E 68th St New York, NY 10065, USA

[2]Département de médecine moléculaire, Université Laval, Québec G1V 0A6, Canada

[3]Axe Neurosciences, Centre de recherche du CHU de Québec, Québec G1V 4G2, Canada

[4]Center for Molecular and Cellular Biology of Inflammation, Division of Immunology, Infection, and Inflammatory Diseases King's College London, London SE1 1UL, United Kingdom

[5]Weill Cornell Graduate School of Medical Sciences, Weill Cornell Medicine, 1300 York Avenue New York, NY 10065, USA

[6]Department of Biology, University of Erlangen-Nuremberg, Erwin-Rommel-Str. 3, 91058 Erlangen, Germany

[7]Howard Hughes Medical Institute, Memorial Sloan-Kettering Cancer Center, 417 East 68th Street, New York, NY 10065, USA

[8]The Feinstein Institute for Medical Research, Manhasset, NY, 11030, USA

[9]Department of Medicine, Recanati Miller Transplant Institute and Immunology Institute, Mount Sinai School of Medicine, New York, NY 10029, USA

[10]Immunotoxicology Team Division, National Institute for Biological Standards and Control, Potters Bar EN6 3QG UK, United Kingdom

SUMMARY

Correspondence: geissmaf@mskcc.org.

Supplemental information

Supplemental Information includes Supplemental Experimental Procedures, six figures, one table, and seven movies.

Author Contributions

EGS and FG designed the study, prepared figures and wrote the draft of the manuscript. EGS performed the majority of experiments, with help from CC, MB, LC and WY. KB and MET performed immuno electron microscopy experiments. DK and FN provided FcγR-deficient mice, characterized expression of FcγRIV in the kidney and the affinity of rabbit immunoglobulins used in the study for Fcγ receptors. XF performed parabiosis surgery. SD prepared albumin-CPG conjugates. PSH provided complement deficient mice and AD provided serum from BXSB-NZW mice. All coauthors contributed to data analysis and revised the manuscript.

Small immune complexes cause type III hypersensitivity reactions that frequently result in tissue injury. The responsible mechanisms however remain unclear and differ depending on target organs. Here we identify a kidney-specific anatomical and functional unit, formed by resident macrophages and peritubular capillary endothelial cells, which monitors the transport of proteins and particles ranging from 20 to 700 kDa or 10 to 200 nm into the kidney interstitium. Kidney resident macrophages detect and scavenge circulating immune complexes ‘pumped’ into the interstitium via trans-endothelial transport, and trigger a FcγRIV-dependent inflammatory response and the recruitment of monocytes and neutrophils. In addition, FcγRIV and TLR pathways synergistically ‘super-activate’ kidney macrophages when immune complexes contain a nucleic acid. These data identify a physiological function of tissue resident kidney macrophages and a basic mechanism by which they initiate the inflammatory response to small immune complexes in the kidney.

Graphical Abstract

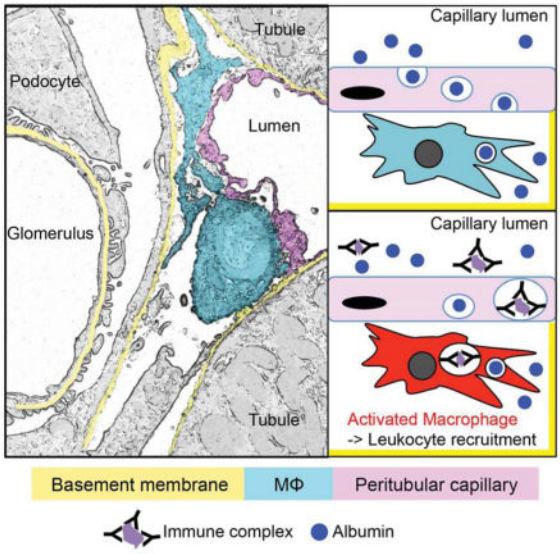

INTRODUCTION

Opsonization of microbial pathogens by immunoglobulins results in immune complexes that are cleared by the innate immune system via binding to Fc receptors (FcRs), complement activation, natural killer (NK)-cell mediated killing, and via phagocytosis by macrophages in the spleen and liver (Bournazos et al., 2015; Guilliams et al., 2014; Nimmerjahn and Ravetch, 2007; Schifferli and Taylor, 1989; Vidarsson and van de Winkel, 1998). However, low molecular weight immune complexes (referred to below as small immune complexes, SIC) are believed to be less efficiently cleared by liver and spleen macrophages, which can result in the activation of neutrophils and monocytes (Jancar and Crespo; Jönsson et al., 2013; Mayadas et al., 2009), complement (Merle et al., 2015), endothelial cells (Sun et al., 2013) and mast cells (Daha et al., 1988). Immune complexes also deposit in tissues, either as a result of increased vascular permeability or tissue damage (Binstadt et al., 2006; Stokol et al., 2004).

Clinical conditions caused by SIC are collectively known as ‘Type III hypersensitivity’ reactions and include the Arthus reaction, serum sickness, post-streptococcal glomerulonephritis, cryoglobulinemia, rheumatoid arthritis, and Systemic Lupus Erythematosus (SLE) (Froehlich and Verma, 2001; Lamprecht et al., 1999; Mayadas et al., 2009; Nimmerjahn and Ravetch, 2007; Schifferli and Taylor, 1989; Vidarsson and van de Winkel, 1998). Type III hypersensitivity can be experimentally induced by immune complexes formed in excess of self and foreign antigens, including proteins, (deoxy)ribo-nucleo-proteins, and drugs. Mice deficient in the activating receptors for the Fc portion of immunoglobulin G (FcγRs) are protected from acute and progressive glomerulonephritis, arthritis, SLE nephritis, and the Arthus reaction (Nimmerjahn and Ravetch, 2008), suggesting that activating FcγRs expressed by cells of the innate immune system play a major role in type III hypersensitivity.

However, the mechanisms that control type III hypersensitivity remain poorly understood, and different mechanisms may mediate the toxicity of SIC in distinct vascular beds. SIC can bind to the endothelium, in particular following complement activation (Daha et al., 1988) and directly trigger increased vascular permeability in vascular beds adjacent to joints, but not the skin or intestine (Binstadt et al., 2006). The Arthus reaction, which results from formation of antigen/antibody complexes *in situ* in the dermis after the intradermal injection of an antigen, is dependent on mast cells, the murine FcγRIII and FcεRI expressed by mast cells, and is independent of FcγRIV and complement (Hazenbos et al., 1996; Nimmerjahn et al., 2010; Sylvestre and Ravetch, 1994; Sylvestre and Ravetch, 1996). In contrast, mast cell deficiency does not modify the pathogenesis of Lupus glomerulonephritis in B6$^{lpr/lpr}$ mice (van Nieuwenhuijze et al., 2015). The murine intermediate/low-affinity IgG receptor FcγRIV - ortholog of human FcγRIIIa (Davis et al., 2002; Mechetina et al., 2002) - expressed by granulocytes, monocytes and macrophages is sufficient for autoantibody-induced nephrotoxic nephritis, rheumatoid arthritis and experimental epidermolysis bullosa acquisita (Kasperkiewicz et al., 2012; Mancardi et al., 2011; Nimmerjahn et al., 2010).

The role of tissue macrophages in type III hypersensitivity is largely unknown, beyond their reported ‘inefficiency’ to clear SIC. Recent progress in the developmental biology of myeloid cells has led to the concept that two lineages of myeloid cells may exert distinct functions within tissues. Resident macrophages, which develop during embryogenesis, are likely to mediate homeostatic ‘housekeeping’ functions, such as the phagocytosis of opsonized particles, while leucocytes that differentiate in the bone marrow and are recruited into tissues from the blood – including neutrophils, monocytes, and dendritic cells – are likely to be primarily involved in the innate immune response (Gomez Perdiguero and Geissmann, 2013; Yamasaki et al., 2014).

To interrogate the respective contribution of resident versus bone marrow (BM)-derived cells to Type III hypersensitivity in mice, we investigated *in vivo* the distribution, kinetics of uptake and responses to SIC by resident macrophages and bone marrow-derived leucocytes. Our data indicate that Kupffer cells (KC) and spleen red pulp macrophages (RPMΦs) rapidly take up circulating SIC as well as large particles, such as 2 μm latex beads, as expected since they are located within sinusoidal (sieved) endothelia and sample the bloodstream. Surprisingly however, the resident macrophage population of the kidney also

takes up circulating SIC as efficiently and rapidly as spleen and liver macrophages, even though it does not take up large circulating beads. SIC uptake by kidney macrophages is mediated by FcγRIV and triggers an inflammatory response that is characterized by cytokine production and is required for the recruitment of blood monocytes and neutrophils. These features appear to be specific to the kidney as dermal macrophages, for example, neither efficiently take up SIC nor mediate an inflammatory response to SIC *in vivo*. We found that this response of kidney macrophages resulted from their unique anatomical location, at the abluminal side of the endothelium of peritubular capillaries, where they actively monitor the trans-endothelial transport of albumin that takes place between the capillaries and the peritubular interstitial space (Bell et al., 1978; Källskog and Wolgast, 1973; Pinter, 1967; Pinter and O'Morchoe, 1970). These data identify a unique property of kidney macrophages, i.e. the immune monitoring of trans-endothelial transport into the kidney interstitium, and provide a mechanism for the initiation of type III hypersensitivity in the kidney and the pathogenesis of kidney damage by small circulating immune complexes.

Results

Kidney macrophages take up circulating small soluble immune complexes (SIC)

To probe uptake of circulating proteins and small immune complexes by tissue macrophages and blood leucocytes *in vivo*, we initially followed the uptake of fluorescent bovine serum albumin (BSA) or chicken ovalbumin (OVA), and small immune complexes (SIC) prepared by incubating rabbit polyclonal immunoglobulin G (IgG) against bovine serum albumin (RaBSA) or chicken ovalbumin (RaOVA) with an excess of BSA or OVA (Clatworthy et al., 2014; Stokol et al., 2004) (Figure S1A). Rabbit IgG bind FcγRI and FcγRIV with K_D of 10^{-7}–10^{-8} and FcγRIIb/III with K_D of 10^{-5}, and ~20% of IgG was bound to albumin to form ~700 kDa SIC (Figures S1A and S1B). Following intravenous (*i.v.*) injection of fluorescent albumin and SIC, fluorescence accumulated in F4/80^{bright} macrophages in the spleen (red pulp macrophages, RPMΦs), the liver (Kupffer cells) and the kidney (Figures 1A and 1B), but there was no detectable uptake of fluorescent albumin or SIC by dermal macrophages, epidermal Langerhans cells, alveolar macrophages and microglia (Figure 1A). Uptake of fluorescent albumin and SIC by kidney, liver and spleen macrophages was time- and dose- dependent, and uptake of SIC was more efficient than uptake of albumin alone (Figures 1C, 1D and S1C–S1F). In contrast, uptake of fluorescent albumin or SIC by monocytes (F4/80^{int}CD11b^{high} cells) and granulocytes (F4/80^{-}CD11b^{high} cells) was not significant (Figures 1B–1D and S1C).

To verify that immune complexes, rather than unbound antibodies, were responsible for the increased uptake of albumin by kidney macrophages, we compared uptake of 'mock' immune complexes (BSA;RaOVA) versus BSA;RaBSA SIC. These experiments indicated that anti-OVA antibodies do not increase BSA uptake (Figure 1E), thus antibody-antigen complexes are required to increase the scavenging by macrophages. Flow cytometry analysis of kidney macrophages following *i.v.* injection of BSA-alexa488;RaBSA and immunostaining with a goat anti-rabbit-alexa555 also indicated that kidney macrophages take up SIC preferentially to albumin alone (Figure S1G).

Intravital microscopy and flow cytometry analysis indicated uptake of SIC by macrophages within vesicular (Figure 1F) and acidic compartments (Figure 1G) as shown by uptake of DQ-BSA;RaBSA (Phan et al., 2009). Following *i.v.* injection of SIC, immunofluorescence on fixed kidney cryosections with antibodies against F4/80 and rabbit IgG showed that the macrophages that take up SIC are located close to endothelial cells, around tubules and around glomeruli (Figures 2A and S2A–S2C, see also Figure 3). We also observed that dense periglomerular and peritubular IgG2a deposits colocalized with F4/80 staining in cryosections from kidneys of autoimmune NZB/W mice, but not wild-type (wt) C57BL/6 mice (Figures 2B and S2D).

These results altogether indicated that Kupffer cells and RPMΦs efficiently take up circulating SIC, and that this is also the case for kidney macrophages in these experimental settings and possibly in 'autoimmune' NZB/W mice. The sinusoidal endothelium of the liver and the spleen red pulp allows for direct contact between Kupffer cells and RPMΦs with the bloodstream (Aird, 2007; Mebius and Kraal, 2005), but this is not the case for kidney macrophages. We thus investigated whether uptake selectively takes place in the kidney, or if blood leucocytes take up SIC and subsequently migrate into the kidney.

Kidney F4/80^{bright} cells are tissue resident macrophages that actively survey the microvascular environment

Kidney F4/80^{bright} macrophages were initially described by Hume and Gordon (Hume and Gordon, 1983) and present with features of both dendritic cells and macrophages (Gottschalk and Kurts, 2015). To further characterize these cells, we analyzed them by flow cytometry, immunofluorescence, intravital confocal microscopy and RNAseq analysis. F4/80^{bright} cells constitute ~ 50% of CD45^{+} cells in the kidney of C57BL/6 mice (Figure S2E) and express MHC class II (I-A), Cx3cr1, and CD11c (Figure S2F) in agreement with previous reports (Cao et al., 2015; Krüger et al., 2004). They also express Fcγ receptors, including FcγRIV in contrast to skin macrophages, microglia and kidney endothelial cells (Figures 2C and S2F–S2H). Analysis of parabiotic mice paired for up to 2 months showed that less than 1% of kidney F4/80^{bright} cells exchange between parabionts, in contrast to blood monocytes (Figure 2D). Accordingly, kidney F4/80^{bright} cells are Ccr2 independent (Figure S2I).

Intravital microscopy of the superficial renal cortex in *Cx3cr1*$^{gfp/+}$ mice confirmed that the resident macrophages form a dense network of interstitial stellate cells in close association with capillaries that surround the tubules and glomeruli (Figure 2E and supplementary movies S1 and S2) (Hume and Gordon, 1983; Soos et al., 2006). Resident macrophages were found to be stationary with their cell bodies not moving over a 5 hour timeframe in >95% of cases (Figures S2J and S2K). They dynamically surveyed the microvascular environment (Figure 2F and supplementary movie S3) using their long (>30 μm) and highly motile filopodia, which extended along the capillary walls and can form phagocytic cups to mediate engulfment of bacteria and fungi (Figures S2L and S2M).

Altogether, these data indicated that F4/80^{bright} Cx3cr1^{gfp+} cells are tissue-resident macrophages and not infiltrating monocytes or bone marrow-derived dendritic cells (Liu et al., 2007), located in the immediate vicinity of the microvasculature, and that actively survey

their environment We therefore investigated the mechanisms that may account for the uptake of circulating SIC.

Kidney resident macrophages are located between the capillary endothelium and the basement membranes of tubules and the Bowman capsule

Although confocal microscopy suggested that resident macrophages are located very close to the lumen of peritubular capillaries (Figure 3A), its resolution is limited. Transmission electron microscopy (TEM) showed that the filopodial extensions of macrophages, immunolabeled with either anti-GFP antibodies in *Cx3cr1*$^{gfp+}$ mice or anti-I-A antibodies in wt mice, are located at the abluminal side of the peritubular capillary, often directly apposed to the abluminal endothelial cell surface and between these endothelial cells and the basement membranes of proximal and distal tubules and the Bowman capsule (Figures 3B–3H and S3A–S3C). These features are distinct from the microanatomy of the dermis, where macrophages are separated from the endothelium by a basement membrane (Freinkel and Woodley, 2001).

Kidney resident macrophages monitor vesicular trans-endothelial transport of proteins

In agreement with classical studies (Milici et al., 1987; Predescu and Palade, 1993; Schubert et al., 2001) TEM revealed that peritubular capillaries are rich in caveolae (Figure 3B), transendothelial channels, and clathrin coated vesicles (CCV) and present with diaphragm-subtended fenestrae (Aird, 2007) (Figures 3B–3G). Ultrastructural analyses performed on the kidney of mice sacrificed 1 minute after *i.v.* injection of BSA-immunogold indicated the presence of immunogold in endothelial caveolae (Figure S4A) as well as in macrophage endosomal compartments (Figure S4A). Intravital confocal imaging confirmed uptake of OVA by macrophages within 1–5 minutes of *i.v.* injection (Figure 4A and supplementary movie S4). This is in accordance with previous studies (see discussion) showing extensive albumin transport from capillaries to the interstitium mediated via caveolae/CCV (Milici et al., 1987; Predescu and Palade, 1993; Schubert et al., 2001). We thus hypothesized that the endothelial/macrophage structure we describe above may allow for the immune monitoring of trans-endothelial transport by the resident kidney macrophages. We therefore quantified the kinetics and morphological aspects of the transport of antibodies and immune complexes from the lumen to the macrophages.

Labeling of perivascular macrophages was detectable by intravital confocal microscopy within minutes after *i.v.* injection of 10 μg of phycoerythrin (PE)- conjugated anti-F4/80 or anti-I-A antibodies (MW ~ 450 kDa, Figure 4B and supplementary movies S5 and S6). This was confirmed by flow cytometry, as >95% of kidney macrophages from mice sacrificed 5 minutes after *i.v.* injection of 10 μg anti-I-A antibody were observed to be labeled *in vivo* (Figure 4C). To distinguish caveolae/CCV mediated transport (Aird, 2007; Stan et al., 1999; Stan et al., 2012) from vascular leakage mediated in response to SIC binding to the endothelium (Binstadt et al., 2006) or the projection of filopodia in the capillary lumen (Cheng et al., 2013), mice were sacrificed 30 seconds after *i.v.* injection of OVA;RaOVA and their kidneys were processed for TEM and labeled with Goat anti Rabbit (GaR) conjugated with gold particles. Quantitative analysis revealed that 10% of gold particles localized to the endothelium. Among these, 96% of gold particles were found within endothelial caveolae/

CCV, while only ~ 4% of gold particles were located nearby cellular junctions or diaphragm-subtended fenestrations (Figures 4D, 4E and S4C). 25% of gold particles were attached to macrophages and observed within their endosomal compartments. 60% of gold particles were localized to the interstitial space or to basement membranes (Figure 4E). Intravital imaging directly showed that kidney macrophages take up 20 nm beads by their motile filopodia (Figure 4F and supplementary movie S7), but we did not observe any filopodia extruded into the capillary lumen by TEM.

To formally investigate whether uptake by macrophages *in vivo* was restricted to circulating particles of a size compatible with trans-endothelial transport, we quantified uptake of 2 μm, 200 nm and 20 nm latex beads injected intravenously. Results indicated that kidney macrophages only take up beads of 200 nm and 20 nm, in contrast to RPMΦs and blood monocytes which are able to take up larger 2 μm beads (Figures 4G and S4D). Finally, to test the possibility that SIC binding to the endothelium may induce vascular leakage we investigated by intravital imaging the extravasation of 70 kDa dextran-TRITC following *i.v.* injection of BSA;RaBSA (Binstadt et al., 2006). We did not observed measurable leakage *in vivo* following BSA;RaBSA injection (Figures 4H and S4E).

Altogether, these results provided strong evidence that antibodies and SIC (~700 kDa) are transcytosed into the kidney interstitium via the transendothelial route of albumin transport (Milici et al., 1987) mediated by caveolae/CCV, and that SIC are immediately scavenged by the kidney resident macrophages. In contrast to Kupffer cells and RPMΦs, which phagocytose large particles and immune complexes from the bloodstream, selective scavenging of SIC by kidney macrophages indicates a function restricted to the survey of endothelial transport and of the kidney interstitium.

Fcgr4-mediated uptake and activation of kidney macrophages by immune complexes

Next we sought to investigate whether Fcγ receptors were required for uptake of SIC by kidney macrophages. We found that FcγRIV is required while FcγRI (CD64) was dispensable (Figures 5A, 5B and S5A). FcγRIV is not expressed by kidney endothelial cells (Figure S2H) and conditional inactivation of the *Fcgr4* gene in hematopoietic cells in $Csf1r^{Cre+};Fcgr4^{f/f}$ and $LysM^{Cre+};Fcgr4^{f/f}$ mice was sufficient to reduce SIC uptake to control levels in kidney macrophages, as well as Kupffer cells (Figures 5A, 5B and S5A). SIC uptake was in contrast independent of *Myd88* or *Trif,* suggesting that scavenging is not dependent on a Toll-like receptor-mediated signal, such as endotoxin (Pandey et al., 2015) (Figure S5B).

These data indicated that FcγRIV mediates scavenging by kidney macrophages of immune complexes that enter the kidney interstitium via trans-endothelial transport. Complexed IgG or immune complexes alone do not elicit an inflammatory response from monocyte-derived macrophages *in vitro* in the absence of a TLR agonist (Sutterwala et al., 1997; Vogelpoel et al., 2014). Nevertheless, we found that SIC uptake *in vivo* caused a rapid FcγRIV-dependent and *Myd88*-independent transcriptional inflammatory response by kidney macrophages (Figures 5C, 5D and S5C). The production of TNF by kidney macrophages was confirmed at the protein level and was strongly reduced in *Fcgr4*-deficient mice but not in *Myd88*-deficient mice (Figures 5E, 5F and S5D). In contrast, *i.v.* injection of SIC did not trigger

TNF production by dermal macrophages (Figure 5G), a finding consistent with the observation that they do not scavenge SIC (Figure 1A). Blood monocytes and granulocytes did not significantly produce TNF either (Figure 5F). Following SIC uptake kidney macrophages also expressed increased levels of activation molecules CD86 and MHCII, in a FcγRIV-dependent and *Myd88*-independent manner (Figure S5E, S5F and S5G).

To test the possibility that macrophage activation may be in part dependent on *in vitro* preparation of SIC (Poteser and Wakabayashi, 2004), we compared the effect of *i.v.* injection of BSA, RaBSA, BSA;RaBSA, non-immune rabbit IgG (Ra-IgG), rabbit anti-mouse albumin (Ra-mAlbumin), rabbit anti-mouse transferrin (Ra- mTransferrin), rabbit anti-mouse IgG (Ra-mIgG) and Ra-mIgG $F(ab')_2$. Macrophage activation and TNF production was observed only in presence of rabbit whole IgG complexed with foreign antigens or directed against mouse albumin, transferrin or IgG (Figures 5H and S5H). Intravenous injection of serum from NZWxBXSB lupus prone mice, containing circulating autoantibodies (Kahn et al., 2008) also resulted in a dose-dependent and FcγRIV-dependent activation of kidney macrophages (Figure 5I). Finally, to investigate whether complement is required for macrophage activation in response to SIC, we analysed *Cfb*-, *C3*-, *C5aR*- and *C5aR/C3aR*-deficient mice injected with rabbit anti-mouse albumin (Ra-mAlbumin, as in Figure 5H). SIC-induced TNF production by macrophages in these animals was not different than in wild-type controls (Figure S5I) suggesting that complement is not required at this stage of macrophage activation.

Altogether these data strongly suggested that circulating SIC access the interstitium through caveolae-mediated transport across the endothelium of peritubular capillaries, where they are scavenged by kidney resident macrophages resulting in FcγRIV-mediated, but *Myd88*- and complement-independent macrophage activation.

Selective recruitment of monocytes and neutrophils in the kidney by SIC-activated resident macrophages

Intravenous injection of SIC also resulted, over the following 6 hours, in a progressive accumulation of $Ly6C^{high}$ monocytes, $Ly6C^{low}$ patrolling monocytes, and neutrophils in the kidney (Figures 6A, 6B and S6A), but not in the dermis (Figure S6B) as quantified by flow cytometry and intravital microscopy. This leucocyte recruitment was abrogated in $Fcgr4^{-/-}$ and $LysM^{Cre+};Fcgr4^{f/f}$ mice (Figure 6A). Intravital imaging confirmed the progressive retention of $Ly6C^{low}$ patrolling monocytes in kidney capillaries over time (Figures S6C–S6F). Blood monocytes and neutrophils express FcγRIV (Nimmerjahn et al., 2005). Therefore to test whether expression of FcγRIV by monocytes and granulocytes was required for their recruitment we transferred wild-type and FcγRIV-deficient leucocytes 1 hour before or 1 hour after SIC injection, and analyzed recruitment 6 hours later. We observed a similar recruitment of wild-type and FcγRIV-deficient monocytes and granulocytes to the kidney (Figure 6C). To investigate whether lymphoid cells were involved in leucocyte recruitment we also performed injection of BSA;RaBSA in $Rag2^{-/-}Il2rg^{-/-}$mice, which lack lymphoid cells (DiSanto et al., 1995; Shinkai et al., 1992). Results indicated that *Rag2* and *Il2rg* are dispensable for the recruitment of monocytes and neutrophils by SIC (Figure 6D). Finally, monocyte recruitment was independent of Myd88

(Figure 6E), although neutrophil recruitment was decreased in *Myd88*-deficient mice (Figure 6F).

These data suggested that SIC trigger the recruitment of monocytes and neutrophils via the FcγRIV-dependent activation of kidney resident macrophages. However, granulocyte recruitment by SIC was in part dependent on *Myd88*. This is compatible with the observation that kidney resident macrophages activated by circulating SIC produce *Il1b*, in a FcγRIV dependent manner, which may be involved in neutrophil recruitment.

Macrophage FcγRIV-mediated inflammatory response synergizes with TLR signaling when SIC contain nucleic acids

To investigate directly the respective roles of Myd88 and FcγRIV signaling in the inflammatory response to SIC, we prepared ovalbumin covalently linked to either CpG oligonucleotides (OVA-CpG), a potent TLR9 agonist (Hemmi et al., 2002) or non-stimulatory GpC oligonucleotides (OVA-GpC) as control (Figure 7A). As expected, *i.v.* injection of OVA-GpC;RaOVA induced FcγRIV-dependent macrophage activation - as evaluated by TNF production, expression of activation markers, and recruitment of monocytes and neutrophils in comparison to OVA-GpC alone (Figures 7B–7G). OVA-CpG on its own induced macrophage activation independently of FcγRIV. Moreover, *i.v.* injection of OVA-CpG;RaOVA resulted in a stronger macrophage activation than OVA-CpG alone or OVA-GpC;RaOVA in wild- type mice, but identical to OVA-CpG alone in FcγRIV-deficient mice (Figures 7B–7G). In this model neutrophil recruitment was mostly attributable to the CpG nucleotide (Figure 7D). These data indicate independent, but additive and even synergistic, effects of FcγRIV-dependent and TLR pathways on the activation of resident macrophages suggesting that *Fcgr4*-dependent activation of resident macrophages by SIC synergises with Myd88 signaling when a TLR activating signal is present.

Discussion

We report here a comprehensive set of studies describing a tissue specific anatomical and functional unit, formed by resident macrophages and peritubular capillary endothelial cells, which monitor the transport of proteins and particles ranging from 20 to 700 kDa or 10 to 200 nm into the kidney interstitium (Figure 7H). This allows kidney resident macrophages to immediately detect potential infectious particles, in this case immune complexes, and to initiate an immune response.

Our observations thus provide a simple model to explain type III hypersensitivity to SIC in the kidney, and show that it is governed by a mechanism distinct from the Arthus reaction in the skin mediated by mast cells (Hazenbos et al., 1996; Nimmerjahn et al., 2010; Sylvestre and Ravetch, 1996). It is also distinct from immune complex-mediated arthritis (Binstadt et al., 2006), from immune complex-mediated peritonitis (Hasenberg et al., 2015) and from immune complex-mediated inflammation in the cremaster muscle (Stokol et al., 2004).

The ‘tissue-specific’ role of macrophages in type III reactions in the kidney can be accounted for by their unique subendothelial location in comparison to the dermis, the relatively selective expression of FcγRIV, the renal blood flow to the kidneys representing

25% of cardiac output, and by the higher surface density of transendothelial channels in the kidney capillary bed and higher albumin transport to the interstitium (Milici et al., 1985). The latter was calculated in classical studies to be of 7.1 ± 1-0 ml. sec^{-1} 10^{-4} in 100 g cortical tissue (Bell et al., 1978), which accounts for the higher concentration of albumin in the interstitium of the kidney cortex (Bell et al., 1978; Källskog and Wolgast, 1973; Pinter, 1967; Pinter and O'Morchoe, 1970), and was proposed to facilitate tubular reabsorption of fluid and small solutes (Milici et al., 1985).

Nevertheless, clearance of the capillary filtrate by perivascular macrophages is not unique to the kidney and was also observed in muscle. Observations by Bruns and Palade established that adventitial macrophages in the rat diaphragm take up ferritin from circulation following *i.v.* injection (Bruns and Palade, 1968). In addition, our observation that transendothelial transport is a rapid process is not unique. The group of G. Palade showed that albumin can be transcytosed within 15 seconds after perfusion in the endothelium and pericapillary spaces of myocardial capillaries (Milici et al., 1987), and more recent work demonstrated 'pumping' of antibody via caveolae across the lung endothelium 10 seconds after *i.v.* injection (Oh et al., 2007).

The present study may also shed some light on the debate about the functional consequences of uptake of SIC or aggregated IgG by macrophages. *In vitro,* complexed IgG or immune complexes alone did not elicit an inflammatory response from monocyte-derived macrophages in the absence of a TLR agonist, and were proposed to serve an anti-inflammatory role (Sutterwala et al., 1997; Vogelpoel et al., 2014). However, *in vivo* studies show in a diversity of models that genetic deletion of activating FcγRs can decrease inflammatory responses in mice (Clynes et al., 1998; Kaneko et al., 2006; Nimmerjahn et al., 2010; Sylvestre and Ravetch, 1994). Our results suggest that *in vivo* and at least in the kidney, SIC and aggregated IgG can indeed initiate an FcγRIV-dependent *Myd88*-independent inflammatory response.

Altogether, our observations identify a physiological 'monitoring' function of tissue resident macrophages in the kidney interstitium, and a simple model to explain how SIC initiate kidney inflammation. Sampling of the capillary filtrate by macrophages is not inflammatory *per se.* However, cognate recognition of SIC by the kidney macrophages mediates increased scavenging and a FcγRIV-dependent cellular immune response, which can synergize with Myd88 signaling when SIC contain nucleic acids. These data may carry significant implications for the understanding and prevention of kidney pathologies mediated by SIC, and possibly other nanometer-sized particles.

Experimental Procedures

Mice

Animal procedures were performed in adherence with the Institutional Review Board (IACUC 15-04-006) at MSKCC. Mice were maintained under SPF conditions. Mouse strains are described in Extended Experimental Procedures.

Antibodies and Reagents

Antibodies used for flow cytometry are described in Extended Experimental Procedures. Chicken ovalbumin (OVA)-alexa555, bovine serum albumin (BSA)-alexa488, BSA-TRITC, DQ Green-BSA, 70kD TRITC-conjugated dextran and carboxylate-modified 2, 0.2 or 0.02 μm beads were purchased from Invitrogen (Carlsbad, CA). Endotoxin-free OVA (Hyglos) was conjugated to CpG 1668 or GpC 1668 oligonucleotides (both from Invivogen) as described in Extended Experimental Procedures. Polyclonal rabbit anti-OVA and polyclonal rabbit anti-BSA were purchased from AbD Serotec and Invitrogen respectively, and their affinity for murine FcγRs was determined with a Biacore X100 biosensor system as previously described (Kao et al., 2015), using a 1:1 Langmuir binding model as rabbits have only one IgG class (Rayner et al., 2013). Immune complexes containing OVA and BSA were prepared *in vitro*, as described in Extended Experimental Procedures, and analyzed by fast protein liquid chromatography using a ÄKTA FPLC system (GE Healthcare Life Sciences). Polyclonal rabbit anti-mouse serum albumin (#600-401-254), polyclonal rabbit anti-mouse transferrin (#600-401-255), polyclonal rabbit anti- mouse IgG (#610-4102) and polyclonal rabbit anti-mouse IgG $F(ab')_2$ (#310-4102) were purchased from Rockland Immunochemicals.

Intravenous injection of Immune complexes, albumin, antibodies, and latex beads

Immune complexes, albumin and antibodies were resuspended in PBS and injected *i.v.* in volume of 100 μl. See also Extended Experimental Procedures.

Flow cytometry

Flow cytometry was performed as described in Extended Experimental Procedures. Data were acquired using a BD LSRFortessa flow cytometer, and analysed using FlowJo 9.5 (Tree Star Inc.).

Intravital Microscopy of the Kidney

Intravital confocal microscopy of kidney was performed as previously described (Auffray et al., 2007; Carlin et al., 2013). Briefly, mice were anesthetized, kept at 37°C and received oxygen (0.5 L/min). The left kidney was surgically exposed after a left flank incision, without removing the renal capsule or interrupting the blood flow. See also Extended Experimental Procedures.

Transmission Electron Microscopy

The full methods for TEM are described in Extended Experimental Procedures. In brief, kidneys were dissected and fixed in 5% acrolein and 4% formaldehyde. Sections were stained for rabbit IgG, Cx3cr1-gfp or MHC-II using gold-conjugated goat anti-rabbit (Nanoprobes) and examined at 80kV with a FEI Tecnai Spirit G2 TEM equipped with an ORCA-HR digital camera (10 MP; Hamamatsu). Peritubular capillaries and their surroundings were randomly photographed at 4,800x or 6,800x, for a total surface of ~10,000 μm^2 sampled in 3 animals, and all the immunogold particles in the pictures were counted.

Statistical Test

Two-tailed unpaired t test was used to calculate statistical significance, using Prism 6 software (GraphPad). p values from unpaired Student's t test are indicated in the figure legends.

Supplementary Material

Refer to Web version on PubMed Central for supplementary material.

Acknowledgments

Authors thank Jayanta Chaudari and Doris Herzlinger for helpful discussion of the manuscript, Antonio Pires da Silva Baptista for help with immunofluorescence, Neil Lipman and the Research Animal Resource Center at MSKCC. This work was supported by the National Cancer Institute of the US National Institutes of Health (P30CA008748), the Ludwig Center at Memorial Sloan Kettering Cancer Center, a Wellcome Trust Senior Investigator award (WT101853MA), and an European Research Council Investigator award (2010-StG-261299) to FG, a PhD fellowship from the Oliver Bird Rheumatism Program to EGS. XF is supported by T32 GM07739 to the Weill Cornell/Rockefeller/Sloan-Kettering Tri-Institutional MD-PhD Program. MET is supported by start-up funds from Université Laval and CHU de Québec. PSH is supported by NIH R01 AI 071185. DK and FN are supported by grants from the German Research Foundation (GK1660, CRC1181-A07).

References

Aird WC. Phenotypic Heterogeneity of the Endothelium: I. Structure, Function, and Mechanisms. Circulation Research. 2007; 100:158–173. [PubMed: 17272818]

Auffray C, Fogg D, Garfa M, Elain G, Join-Lambert O, Kayal S, Sarnacki S, Cumano A, Lauvau G, Geissmann F. Monitoring of blood vessels and tissues by a population of monocytes with patrolling behavior. Science. 2007; 317:666–670. [PubMed: 17673663]

Bell DR, Pinter GG, Wilson PD. Albumin permeability of the peritubular capillaries in rat renal cortex. The Journal of Physiology. 1978; 279:621–640. [PubMed: 671365]

Binstadt BA, Patel PR, Alencar H, Nigrovic PA, Lee DM, Mahmood U, Weissleder R, Mathis D, Benoist C. Particularities of the vasculature can promote the organ specificity of autoimmune attack. Nat Immunol. 2006; 7:284–292. [PubMed: 16444258]

Bournazos S, DiLillo DJ, Ravetch JV. The role of Fc–FcγR interactions in IgG-mediated microbial neutralization. The Journal of Experimental Medicine. 2015; 212:1361–1369. [PubMed: 26282878]

Bruns RR, Palade GE. STUDIES ON BLOOD CAPILLARIES: II. Transport of Ferritin Molecules across the Wall of Muscle Capillaries. The Journal of Cell Biology. 1968; 37:277–299. [PubMed: 5656395]

Cao Q, Wang Y, Wang XM, Lu J, Lee VWS, Ye Q, Nguyen H, Zheng G, Zhao Y, Alexander SI, et al. Renal F4/80+CD11c+ Mononuclear Phagocytes Display Phenotypic and Functional Characteristics of Macrophages in Health and in Adriamycin Nephropathy. Journal of the American Society of Nephrology. 2015; 26:349–363. [PubMed: 25012165]

Carlin LM, Stamatiades EG, Auffray C, Hanna RN, Glover L, Vizcay-Barrena G, Hedrick CC, Cook HT, Diebold S, Geissmann F. Nr4a1-dependent Ly6C(low) monocytes monitor endothelial cells and orchestrate their disposal. Cell. 2013; 153:362–375. [PubMed: 23582326]

Cheng LE, Hartmann K, Roers A, Krummel MF, Locksley RM. Perivascular mast cells dynamically probe cutaneous blood vessels to capture immunoglobulin E. Immunity. 2013; 38:166–175. [PubMed: 23290520]

Clatworthy MR, Aronin CEP, Mathews RJ, Morgan NY, Smith KGC, Germain RN. Immune complexes stimulate CCR7-dependent dendritic cell migration to lymph nodes. Nat Med. 2014; 20:1458–1463. [PubMed: 25384086]

Clynes R, Dumitru C, Ravetch JV. Uncoupling of immune complex formation and kidney damage in autoimmune glomerulonephritis. Science. 1998; 279:1052–1054. [PubMed: 9461440]

Daha MR, Miltenburg AM, Hiemstra PS, Klar-Mohamad N, Van Es LA, Van Hinsbergh VW. The complement subcomponent C1q mediates binding of immune complexes and aggregates to endothelial cells in vitro. European journal of immunology. 1988; 18:783–787. [PubMed: 3259929]

Davis RS, Dennis G jr, Odom MR, Gibson AW, Kimberly RP, Burrows PD, Cooper MD. Fc receptor homologs: newest members of a remarkably diverse Fc receptor gene family. Immunological Reviews. 2002; 190:123–136. [PubMed: 12493010]

DiSanto JP, Muller W, Guy-Grand D, Fischer A, Rajewsky K. Lymphoid development in mice with a targeted deletion of the interleukin 2 receptor gamma chain. Proceedings of the National Academy of Sciences of the United States of America. 1995; 92:377–381. [PubMed: 7831294]

Freinkel, RK.; Woodley, DT. The Biology of the Skin. CRC Press; 2001.

Froehlich H, Verma R. Arthus Reaction to Recombinant Hepatitis B Virus Vaccine. Clinical Infectious Diseases. 2001; 33:906–908. [PubMed: 11512098]

Gomez Perdiguero E, Geissmann F. Myb-Independent Macrophages: A Family of Cells That Develops with Their Tissue of Residence and Is Involved in Its Homeostasis. Cold Spring Harbor Symposia on Quantitative Biology. 2013

Gottschalk C, Kurts C. The debate about dendritic cells and macrophages in the kidney. Frontiers in Immunology. 2015; 6

Guilliams M, Bruhns P, Saeys Y, Hammad H, Lambrecht BN. The function of Fc[gamma] receptors in dendritic cells and macrophages. Nat Rev Immunol. 2014; 14:94–108. [PubMed: 24445665]

Hasenberg A, Hasenberg M, Mann L, Neumann F, Borkenstein L, Stecher M, Kraus A, Engel DR, Klingberg A, Seddigh P, et al. Catchup: a mouse model for imaging-based tracking and modulation of neutrophil granulocytes. Nat Meth. 2015; 12:445–452.

Hazenbos WLW, Gessner JE, Hofhuis FMA, Kuipers H, Meyer D, Heijnen IAFM, Schmidt RE, Sandor M, Capel PJA, Daëron M, et al. Impaired IgG-Dependent Anaphylaxis and Arthus Reaction in FcγRIII (CD16) Deficient Mice. Immunity. 1996; 5:181–188. [PubMed: 8769481]

Hemmi H, Kaisho T, Takeuchi O, Sato S, Sanjo H, Hoshino K, Horiuchi T, Tomizawa H, Takeda K, Akira S. Small anti-viral compounds activate immune cells via the TLR7 MyD88-dependent signaling pathway. Nat Immunol. 2002; 3:196–200. [PubMed: 11812998]

Hume DA, Gordon S. Mononuclear phagocyte system of the mouse defined by immunohistochemical localization of antigen F4/80. Identification of resident macrophages in renal medullary and cortical interstitium and the juxtaglomerular complex. The Journal of experimental medicine. 1983; 157:1704–1709. [PubMed: 6854206]

Jancar S, Crespo MS. Immune complex-mediated tissue injury: a multistep paradigm. Trends in Immunology. 26:48–55. [PubMed: 15629409]

Jönsson F, Mancardi DA, Albanesi M, Bruhns P. Neutrophils in local and systemic antibody-dependent inflammatory and anaphylactic reactions. Journal of Leukocyte Biology. 2013; 94:643–656. [PubMed: 23532517]

Kahn P, Ramanujam M, Bethunaickan R, Huang W, Tao H, Madaio MP, Factor SM, Davidson A. Prevention of Murine Antiphospholipid Syndrome by BAFF Blockade. Arthritis and rheumatism. 2008; 58:2824–2834. [PubMed: 18759321]

Källskog Ö, Wolgast M. Driving Forces over the Peritubular Capillary Membrane in the Rat Kidney during Antidiuresis and Saline Expansion. Acta Physiologica Scandinavica. 1973; 89:116–125. [PubMed: 4761515]

Kaneko Y, Nimmerjahn F, Madaio MP, Ravetch JV. Pathology and protection in nephrotoxic nephritis is determined by selective engagement of specific Fc receptors. The Journal of experimental medicine. 2006; 203:789–797. [PubMed: 16520389]

Kao D, Danzer H, Collin M, Groß A, Eichler J, Stambuk J, Lauc G, Lux A, Nimmerjahn F. A Monosaccharide Residue Is Sufficient to Maintain Mouse and Human IgG Subclass Activity and Directs IgG Effector Functions to Cellular Fc Receptors. Cell Reports. 2015; 13:2376–2385. [PubMed: 26670049]

Kasperkiewicz M, Nimmerjahn F, Wende S, Hirose M, Iwata H, Jonkman MF, Samavedam U, Gupta Y, Möller S, Rentz E, et al. Genetic identification and functional validation of FcγRIV as key

molecule in autoantibody-induced tissue injury. The Journal of Pathology. 2012; 228:8–19. [PubMed: 22430937]

Krüger T, Benke D, Eitner F, Lang A, Wirtz M, Hamilton-Williams EE, Engel D, Giese B, Müller-Newen G, Floege J, et al. Identification and Functional Characterization of Dendritic Cells in the Healthy Murine Kidney and in Experimental Glomerulonephritis. Journal of the American Society of Nephrology. 2004; 15:613–621. [PubMed: 14978163]

Lamprecht P, Gause A, Gross WL. Cryoglobulinemic vasculitis. Arthritis & Rheumatism. 1999; 42:2507–2516. [PubMed: 10615995]

Liu K, Waskow C, Liu X, Yao K, Hoh J, Nussenzweig M. Origin of dendritic cells in peripheral lymphoid organs of mice. Nat Immunol. 2007; 8:578–583. [PubMed: 17450143]

Mancardi DA, Jönsson F, Iannascoli B, Khun H, Van Rooijen N, Huerre M, Daëron M, Bruhns P. Cutting Edge: The Murine High-Affinity IgG Receptor FcγRIV Is Sufficient for Autoantibody-Induced Arthritis. The Journal of Immunology. 2011; 186:1899–1903. [PubMed: 21248252]

Mayadas TN, Tsokos GC, Tsuboi N. Mechanisms of Immune Complex Mediated Neutrophil Recruitment and Tissue Injury. Circulation. 2009; 120:2012–2024. [PubMed: 19917895]

Mebius RE, Kraal G. Structure and function of the spleen. Nat Rev Immunol. 2005; 5:606–616. [PubMed: 16056254]

Mechetina LV, Najakshin AM, Alabyev BY, Chikaev NA, Taranin AV. Identification of CD16-2, a novel mouse receptor homologous to CD16/Fc gamma RIII. Immunogenetics. 2002; 54:463–468. [PubMed: 12389094]

Merle N, Church SE, Fremeaux-Bacchi V, Roumenina LT. Complement system part I - molecular mechanisms of activation and regulation. Frontiers in Immunology. 2015; 6

Milici AJ, L'Hernault N, Palade GE. Surface densities of diaphragmed fenestrae and transendothelial channels in different murine capillary beds. Circulation Research. 1985; 56:709–717. [PubMed: 2581719]

Milici AJ, Watrous NE, Stukenbrok H, Palade GE. Transcytosis of albumin in capillary endothelium. The Journal of Cell Biology. 1987; 105:2603–2612. [PubMed: 3320050]

Nimmerjahn F, Bruhns P, Horiuchi K, Ravetch JV. FcγRIV: A Novel FcR with Distinct IgG Subclass Specificity. Immunity. 2005; 23:41–51. [PubMed: 16039578]

Nimmerjahn F, Lux A, Albert H, Woigk M, Lehmann C, Dudziak D, Smith P, Ravetch JV. FcγRIV deletion reveals its central role for IgG2a and IgG2b activity in vivo. Proceedings of the National Academy of Sciences. 2010; 107:19396–19401.

Nimmerjahn F, Ravetch JV. Fc-receptors as regulators of immunity. Adv Immunol. 2007; 96:179–204. [PubMed: 17981207]

Nimmerjahn F, Ravetch JV. Fc[gamma] receptors as regulators of immune responses. Nat Rev Immunol. 2008; 8:34–47. [PubMed: 18064051]

Oh P, Borgstrom P, Witkiewicz H, Li Y, Borgstrom BJ, Chrastina A, Iwata K, Zinn KR, Baldwin R, Testa JE, et al. Live dynamic imaging of caveolae pumping targeted antibody rapidly and specifically across endothelium in the lung. Nat Biotech. 2007; 25:327–337.

Pandey S, Kawai T, Akira S. Microbial sensing by Toll-like receptors and intracellular nucleic acid sensors. Cold Spring Harb Perspect Biol. 2015; 7:a016246. [PubMed: 25301932]

Phan TG, Green JA, Gray EE, Xu Y, Cyster JG. Immune complex relay by subcapsular sinus macrophages and noncognate B cells drives antibody affinity maturation. Nat Immunol. 2009; 10:786–793. [PubMed: 19503106]

Pinter GG. Distribution of chylomicrons and albumin in dog kidney. The Journal of Physiology. 1967; 192:761–772. [PubMed: 6059001]

Pinter GG, O'Morchoe CC. Turnover of interstitial albumin in the kidney. Experientia. 1970; 26:265–266. [PubMed: 5417488]

Poteser M, Wakabayashi I. Serum albumin induces iNOS expression and NO production in RAW 267.4 macrophages. British Journal of Pharmacology. 2004; 143:143–151. [PubMed: 15289288]

Predescu D, Palade GE. Plasmalemmal vesicles represent the large pore system of continuous microvascular endothelium. American Journal of Physiology - Heart and Circulatory Physiology. 1993; 265:H725–H733.

Rayner LE, Kadkhodayi-Kholghi N, Heenan RK, Gor J, Dalby PA, Perkins SJ. The Solution Structure of Rabbit IgG Accounts for Its Interactions with the Fc Receptor and Complement C1q and Its Conformational Stability. Journal of Molecular Biology. 2013; 425:506–523. [PubMed: 23178865]

Schifferli JA, Taylor RP. Physiological and pathological aspects of circulating immune complexes. Kidney Int. 1989; 35:993–1003. [PubMed: 2651776]

Schubert W, Frank PG, Razani B, Park DS, Chow CW, Lisanti MP. Caveolae-deficient Endothelial Cells Show Defects in the Uptake and Transport of Albumin in Vivo. Journal of Biological Chemistry. 2001; 276:48619–48622. [PubMed: 11689550]

Shinkai Y, Rathbun G, Lam KP, Oltz EM, Stewart V, Mendelsohn M, Charron J, Datta M, Young F, Stall AM, et al. RAG-2-deficient mice lack mature lymphocytes owing to inability to initiate V(D)J rearrangement. Cell. 1992; 68:855–867. [PubMed: 1547487]

Soos TJ, Sims TN, Barisoni L, Lin K, Littman DR, Dustin ML, Nelson PJ. CX3CR1+ interstitial dendritic cells form a contiguous network throughout the entire kidney. Kidney Int. 2006; 70:591–596. [PubMed: 16760907]

Stan RV, Kubitza M, Palade GE. PV-1 is a component of the fenestral and stomatal diaphragms in fenestrated endothelia. Proceedings of the National Academy of Sciences. 1999; 96:13203–13207.

Stan, Radu V.; Tse, D.; Deharvengt, Sophie J.; Smits, Nicole C.; Xu, Y.; Luciano, Marcus R.; McGarry, Caitlin L.; Buitendijk, M.; Nemani, Krishnamurthy V.; Elgueta, R., et al. The Diaphragms of Fenestrated Endothelia: Gatekeepers of Vascular Permeability and Blood Composition. Developmental Cell. 2012; 23:1203–1218. [PubMed: 23237953]

Stokol T, O'Donnell P, Xiao L, Knight S, Stavrakis G, Botto M, von Andrian UH, Mayadas TN. C1q Governs Deposition of Circulating Immune Complexes and Leukocyte Fcγ Receptors Mediate Subsequent Neutrophil Recruitment. The Journal of Experimental Medicine. 2004; 200:835–846. [PubMed: 15466618]

Sun W, Jiao Y, Cui B, Gao X, Xia Y, Zhao Y. Immune complexes activate human endothelium involving the cell-signaling HMGB1-RAGE axis in the pathogenesis of lupus vasculitis. Lab Invest. 2013; 93:626–638. [PubMed: 23628898]

Sutterwala FS, Noel GJ, Clynes R, Mosser DM. Selective Suppression of Interleukin-12 Induction after Macrophage Receptor Ligation. The Journal of Experimental Medicine. 1997; 185:1977–1985. [PubMed: 9166427]

Sylvestre D, Ravetch J. Fc receptors initiate the Arthus reaction: redefining the inflammatory cascade. Science. 1994; 265:1095–1098. [PubMed: 8066448]

Sylvestre DL, Ravetch JV. A Dominant Role for Mast Cell Fc Receptors in the Arthus Reaction. Immunity. 1996; 5:387–390. [PubMed: 8885871]

van Nieuwenhuijze AE, Cauwe B, Klatt D, Humblet-Baron S, Liston A. Lpr-induced systemic autoimmunity is unaffected by mast cell deficiency. Immunol Cell Biol. 2015; 93:841–848. [PubMed: 25849740]

Vidarsson G, van de Winkel JG. Fc receptor and complement receptor-mediated phagocytosis in host defence. Curr Opin Infect Dis. 1998; 11:271–278. [PubMed: 17033391]

Vogelpoel LTC, Hansen IS, Rispens T, Muller FJM, van Capel TMM, Turina MC, Vos JB, Baeten DLP, Kapsenberg ML, de Jong EC, et al. Fc gamma receptor-TLR cross-talk elicits pro-inflammatory cytokine production by human M2 macrophages. Nat Commun. 2014; 5

Yamasaki R, Lu H, Butovsky O, Ohno N, Rietsch AM, Cialic R, Wu PM, Doykan CE, Lin J, Cotleur AC, et al. Differential roles of microglia and monocytes in the inflamed central nervous system. The Journal of Experimental Medicine. 2014; 211:1533–1549. [PubMed: 25002752]

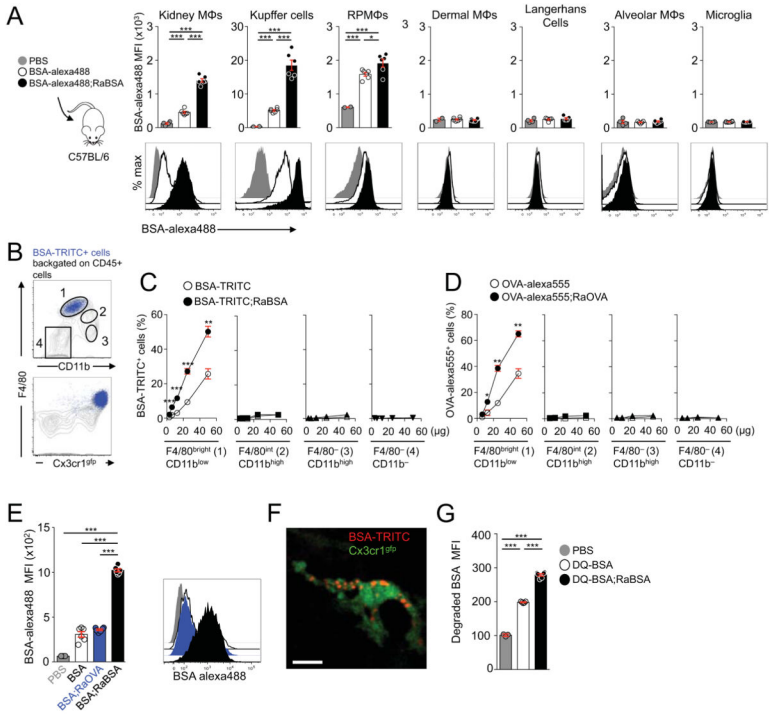

Figure 1. Uptake of immune complexes by kidney macrophages

(A) Flow cytometric analysis of BSA-alexa488 uptake by macrophages from C57BL/6 mice injected *i.v.* with 50 μg BSA-alexa488 or BSA-alexa488;RaBSA (50 μg BSA-alexa488 + 110 μg RaBSA) 2 hours prior to analysis. Scatter plots (top: geometric mean fluorescent intensity, MFI) and representative histograms (bottom) N = 2–6 mice per treatment. **(B)** Uptake of BSA-TRITC by kidneys leukocytes from *Cx3cr1*$^{gfp/+}$mice injected *i.v.* with BSA-TRITC;RaBSA (50 μg BSA-TRITC + 110 μg RaBSA) 2 hours prior to analysis. Plots are representative of 10 mice. **(C)** Uptake of BSA-TRITC as in (B) by kidney leukocytes in *Cx3cr1*$^{gfp/+}$ *Rag2*$^{-/-}$ *Il2rg*$^{-/-}$ mice 2 hours after *i.v.* injection of increasing amounts of BSA-TRITC or BSA-TRITC;RaBSA. N = 2–6 mice per treatment, per dose. **(D)** As in (C) for increasing amounts of OVA-alexa555 or OVA-alexa555;RaOVA. N = 2–8 mice per treatment, per dose. **(E)** BSA-alexa488 uptake by kidney F4/80^{bright} macrophages injected *i.v.* with PBS, 50 μg BSA-alexa488, BSA-alexa488;RaOVA or BSA-alexa488;RaBSA 2 hours prior to analysis as in (A). N = 3–6 mice per treatment. **(F)** Still frame from intravital imaging (IVM) of the superficial renal cortex of a *Cx3cr1*$^{gfp/+}$ mouse 2 hours after *i.v.* injection of 50 μg BSA-TRITC;RaBSA as in (C). N = 10 mice. Bar = 10 μm. **(G)** Flow cytometric analysis of DQ-BSA fluorescence in kidney F4/80^{bright} macrophages 2 hours after *i.v.* injection of 12.5 μg DQ-BSA or DQ-BSA;RaBSA (12.5 μg DQ-BSA + 27.5 μg RaBSA). N = 3–6 mice per treatment. Bars indicate mean value ± S.E.M. Symbols represent individual mice. *P < 0.05, **P < 0.01, ***P < 0.001 using a two-tailed, unpaired t-test. See also Figure S1.

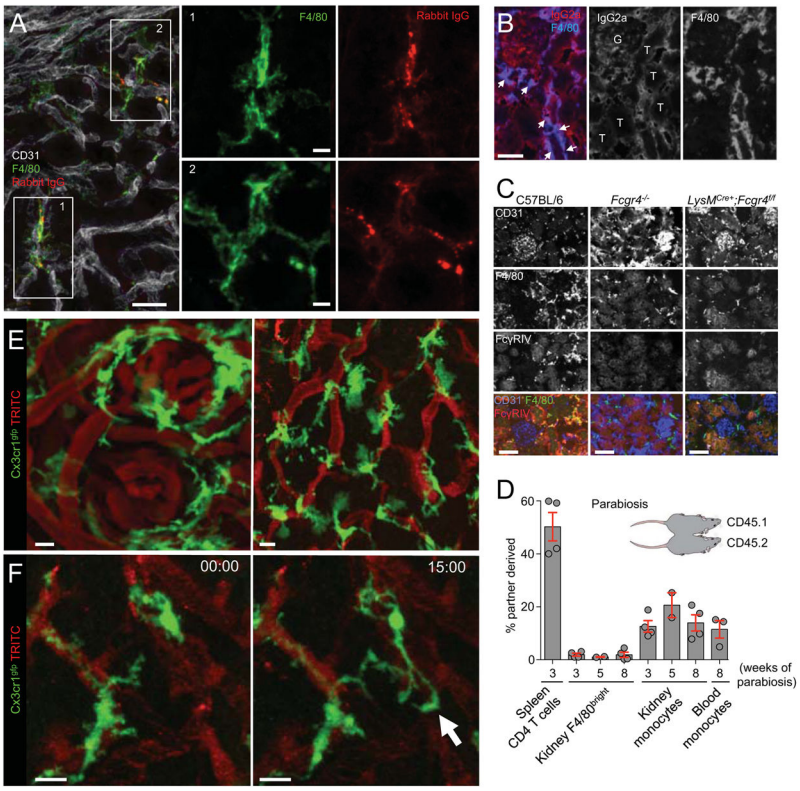

Figure 2. Kidney F4/80^{bright} cells are tissue resident macrophages

(A) Immunofluorescence (IF) staining for F4/80, CD31 and rabbit IgG in kidney cryosections from a C57BL/6 mouse injected *i.v.* with BSA;RaBSA (50 μg BSA + 110 μg RaBSA) 2 hours prior to euthanasia. N = 3 mice. **(B)** IF staining for F4/80 and mouse IgG2a in kidney cryosections from a 6-month old NZBxW F1 mouse. G, glomerulus; T, tubule. Arrows indicate co-localistion of F4/80 and IgG2a staining. **(C)** IF staining for F4/80, CD31 and FcγRIV in kidney cryosections from C57BL/6, *Fcgr4*$^{-/-}$ and *LysM*$^{Cre+}$*;Fcgr4*$^{f/f}$ mice. **(D)** CD45.1 and CD45.2 congenic mice analyzed on 3, 5 or 8 weeks of parabiosis. Histograms represents percentage of partner-derived cells in the spleen, kidney and blood. N = 2–4 parabionts per time point. Bars indicate mean value ± S.E.M. Symbols represent individual mice. **(E–F)** Still frames from IVM of the superficial renal cortex in *Cx3cr1*$^{gfp/+}$ *Rag2*$^{-/-}$ *Il2rg*$^{-/-}$ mice. Capillaries are visualized by *i.v.* injection of 70 kDa dextran-TRITC. Arrow in (F) indicates macrophage filopodial extension. Time in (F) is shown in min:sec. Bars = 10 μm (A, E, F) or 50 μm (B, C). See also Figure S2 and supplementary movies S1–S3.

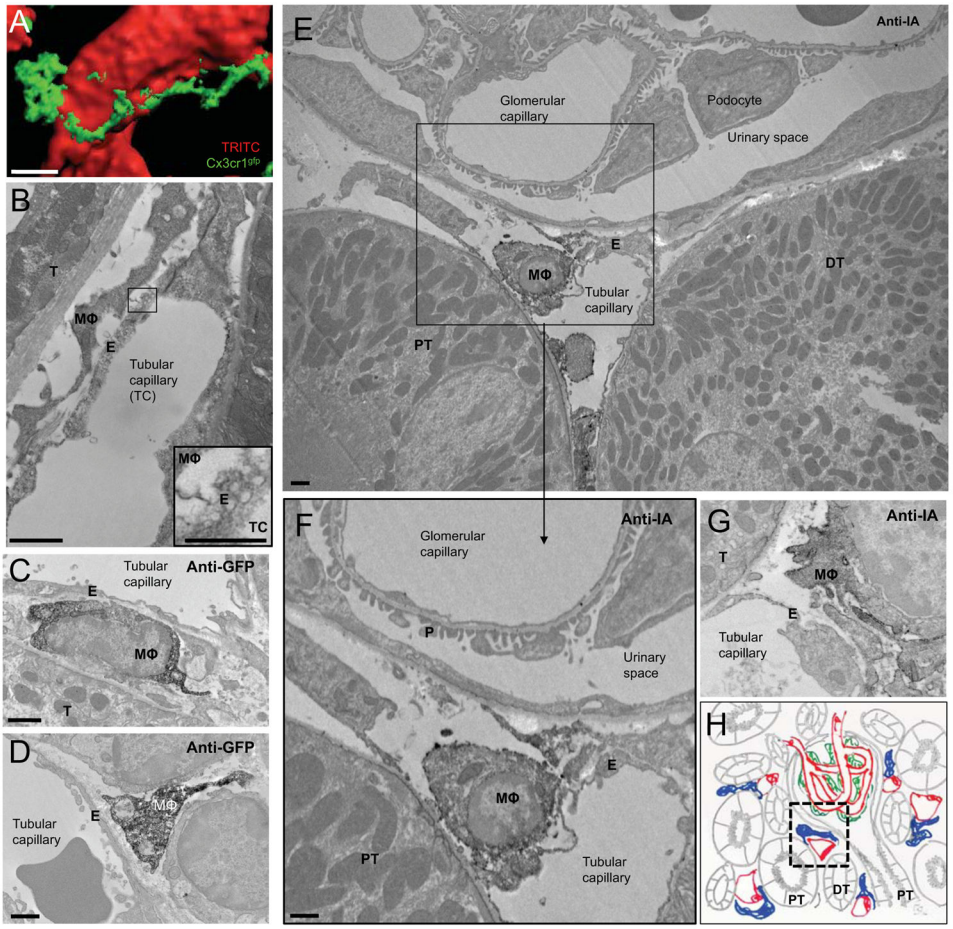

Figure 3. Kidney resident macrophages are located between the capillary endothelium and the basement membranes of tubules and the Bowman capsule

(A) 3D surface rendering of a still frame form IVM of the kidney in a *Cx3cr1*$^{gfp/+}$ *Rag2*$^{-/-}$ *Il2rg*$^{-/-}$ mouse. Cx3cr1^{gfp} macrophage is in green. Capillaries (red) are visualized in red by *i.v.* injection of 70 kDa dextran-TRITC. **(B)** Transmission Electron Microscopy (TEM) image of the kidney cortex from a C57BL/6 mouse. MΦ: macrophage, E: endothelium, T: tubule. Inset shows endothelial plasmalemmal vesicles. **(C–D)** TEM images of the renal cortex in a *Cx3cr1*$^{gfp/+}$ mouse immunostained for GFP. MΦ: macrophage, E: endothelium, T: tubule. **(E–G)** TEM images of the renal cortex in a C57BL/6 mouse immunostained for I-A. MΦ: macrophage, E: endothelium, PT: proximal tubule, DT: distal tubule, T: tubule, P: podocyte foot processes. Bars = 10 μm (A), 1 μm (B–H), 0.5 μm (inset in B). See also Figure S3. **(H)** Scheme giving the anatomical context of EM pictures. Capillaries are depicted in red, macrophage in blue, podocytes in green and epithelial structures in grey, PT: proximal tubule, DT: distal tubule. The area corresponding to EM pictures in E and F is indicated by a dashed black line.

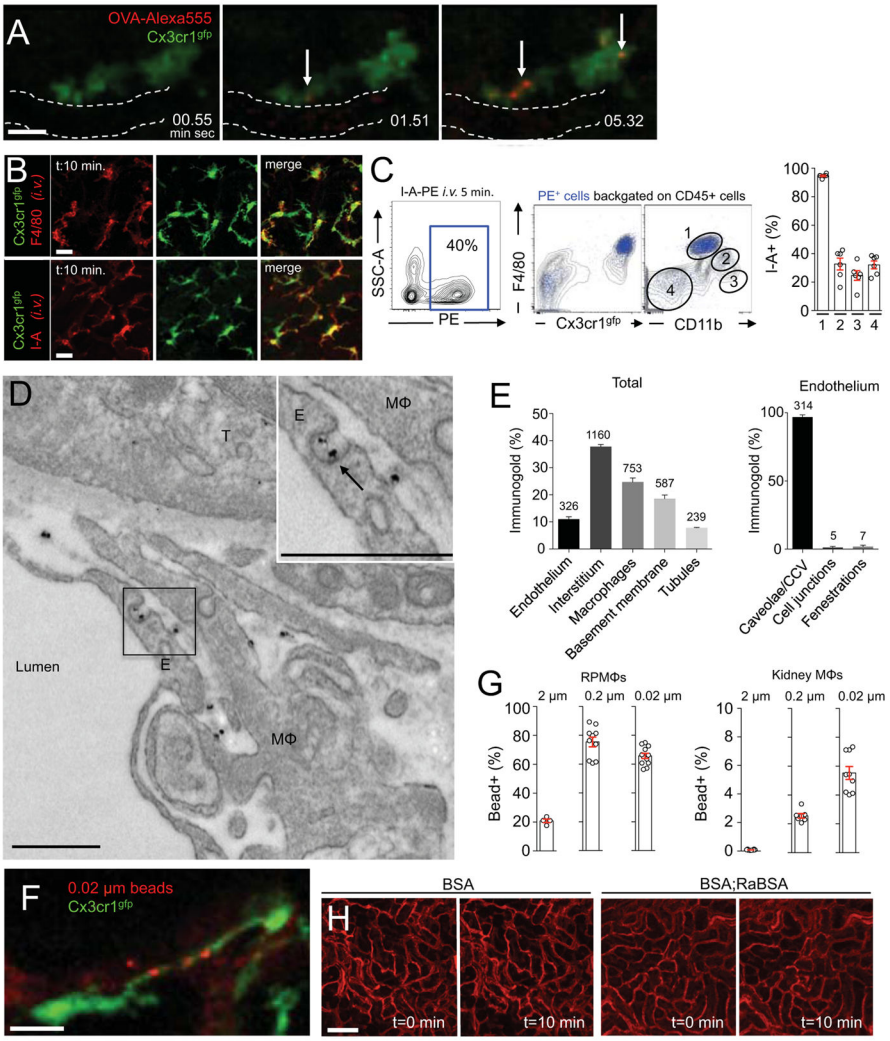

Figure 4. Macrophages monitor transendothelial transport of circulating immune complexes

(A) Still frames from IVM of the kidney from *Cx3cr1*$^{gfp/+}$ mouse receiving 50 μg OVA-alexa555 *i.v.*. Arrows indicate OVA-positive macrophage. Time is min:sec from the time of *i.v.* injection. Bar = 10 μm. **(B)** As in (A) 10 minutes after *i.v.* injection of 10 μg PE-conjugated antibodies against F4/80 (top) and I-A (bottom). Bars = 20 μm. N = 3–4 mice per antibody. **(C)** Flow cytometry analysis of kidney leucocytes from *Cx3cr1*$^{gfp/+}$ mice sacrificed 5 minutes after *i.v.* injection of 10 μg anti-I-A. N = 6 mice. **(D)** TEM of the kidney cortex from mice sacrificed 30 seconds after *i.v.* injection of OVA;RaOVA. RaOVA is detected with gold-conjugated goat anti-rabbit. Arrow indicates gold particles in endothelial caveolae/CCV. Macrophages are identified by immunocytochemistry for I-A. MΦ: macrophage, E: endothelium, T: tubule. Bars = 0.5 μm. **(E)** Quantification of total (left) and endothelium-associated (right) immunogold particles in mice treated in (D). The numbers above bars indicate the absolute number of gold particles counted in total N = 3 mice. **(F)** Still frame from IVM of phagocytosis of 0.02 μm beads by a kidney macrophage in *Cx3cr1*$^{gfp/+}$ mice. Bar = 10 μm. **(G)** Phagocytosis of 2, 0.2 and 0.02 μm beads by splenic RPMΦs (left) and kidney macrophages (right) 2 hours after *i.v.* injection. N = 5–12 per

treatment. **(H)** Still frames from IVM of the superficial renal cortex in C57BL/6 mice injected *i.v.* with 70 kDa dextran-TRITC to label the vascular bed (red), and 5–7 min later, with BSA, or BSA;RaBSA (50 μg/mouse). Images are shown immediately before and 10 minutes after injection of BSA, or BSA;RaBSA. Bars = 100 μm. Each symbol in (C) and (G) represents an individual mouse. See also Figure S4 and supplementary movies S4–S7.

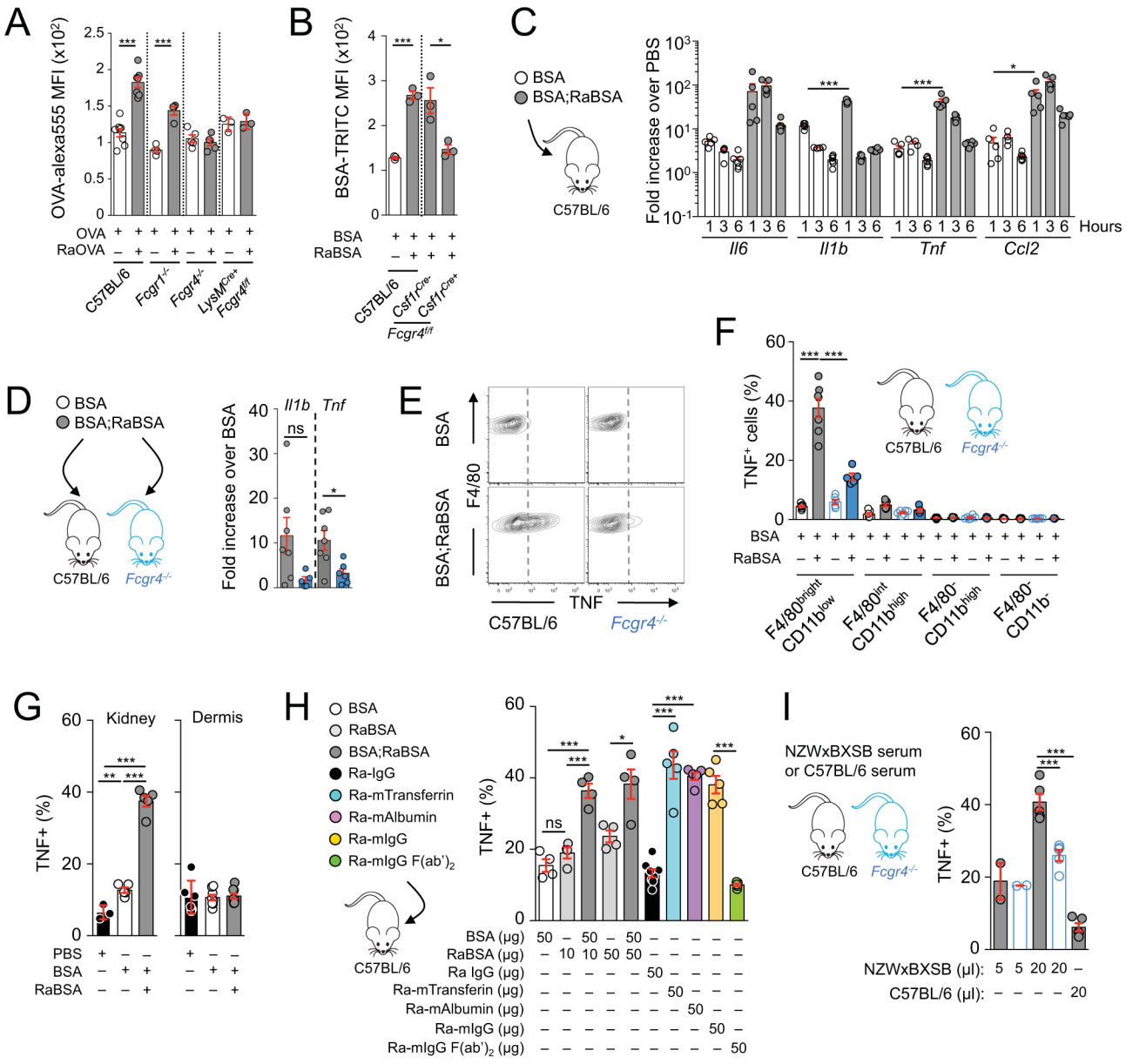

Figure 5. FcγRIV-dependent uptake and activation of kidney, but not dermal, macrophages by small immune complexes, 'auto' antibodies, and NZWxBXSB serum

(A) Uptake of OVA-alexa555 by kidney macrophages from *wt*, *Fcgr1*$^{-/-}$, *Fcgr4*$^{-/-}$ and *LysM*$^{Cre+}$;*Fcgr4*$^{f/f}$ mice 2 hours after *i.v.* injection of 6.5 µg OVA-alexa555 or OVA-alexa555;RaOVA (6.5 µg OVA-alexa555 + 21.25 µg RaOVA). N = 3–7 mice per treatment, per genotype. **(B)** Uptake of BSA-TRITC by kidney F4/80^{bright} macrophages from *wt*, *Csf1r*$^{Cre+}$;*Fcgr4*$^{f/f}$ and *Csf1r*$^{Cre-}$;*Fcgr4*$^{f/f}$ mice 2 hours after *i.v.* injection of 50 µg BSA-TRITC or BSA-TRITC;RaBSA. N = 3 mice per treatment, per genotype. **(C)** qPCR analysis of IL-6, Il-1b, Tnf, Ccl2 transcripts in total kidney tissue from C57BL/6 mice 1, 3, and 6 hrs after *i.v.* injection of 50 µg BSA-TRITC or BSA-TRITC;RaBSA. N = 4–6 mice per treatment, per time point. **(D)** qPCR for *Tnf* and *Il1b* in FACS-sorted kidney F4/80^{bright} macrophages from *wt* (C57BL/6) and *Fcgr4*$^{-/-}$ mice 1 hour after treatment. N = 6–7 mice

per treatment, per genotype. **(E–F)** Representative plots (E) and quantification (F) of intracellular staining for TNF in kidney F4/80^{bright} macrophages from *wt* and *Fcgr4*$^{-/-}$ mice 1 hour after treated as in (D). N = 5–7 mice per treatment, per genotype. **(G)** TNF staining in kidney and dermal F4/80^{bright} macrophages from *wt* mice 1 hour after treatment as in (D). N = 3–8 mice per treatment. **(H)** TNF staining in kidney F4/80^{bright} macrophages from *wt* mice 1 hour after *i.v.* injection of the indicated amounts of BSA, RaBSA, BSA;RaBSA, rabbit IgG (Ra-IgG), rabbit anti-mouse transferrin (Ra-mTransferrin), rabbit anti-mouse albumin (Ra-mAlbumin), rabbit anti-mouse IgG (Ra-mIgG) or Ra- mIgG (Fab′)$_2$. N = 4–5 mice per treatment. **(I)** TNF staining in kidney F4/80^{bright} macrophages from *wt* or *Fcgr4*$^{-/-}$ mice 1 hour after *i.v.* injection of increasing amounts of serum from the indicated mouse strains. N = 2–5 mice per dose per genotype. Bars indicate mean value ± S.E.M. Each symbol represents an individual mouse. *P < 0.05, **P < 0.01, ***P < 0.001 using a two-tailed, unpaired t-test. NS, not significant. See also Figure S5.

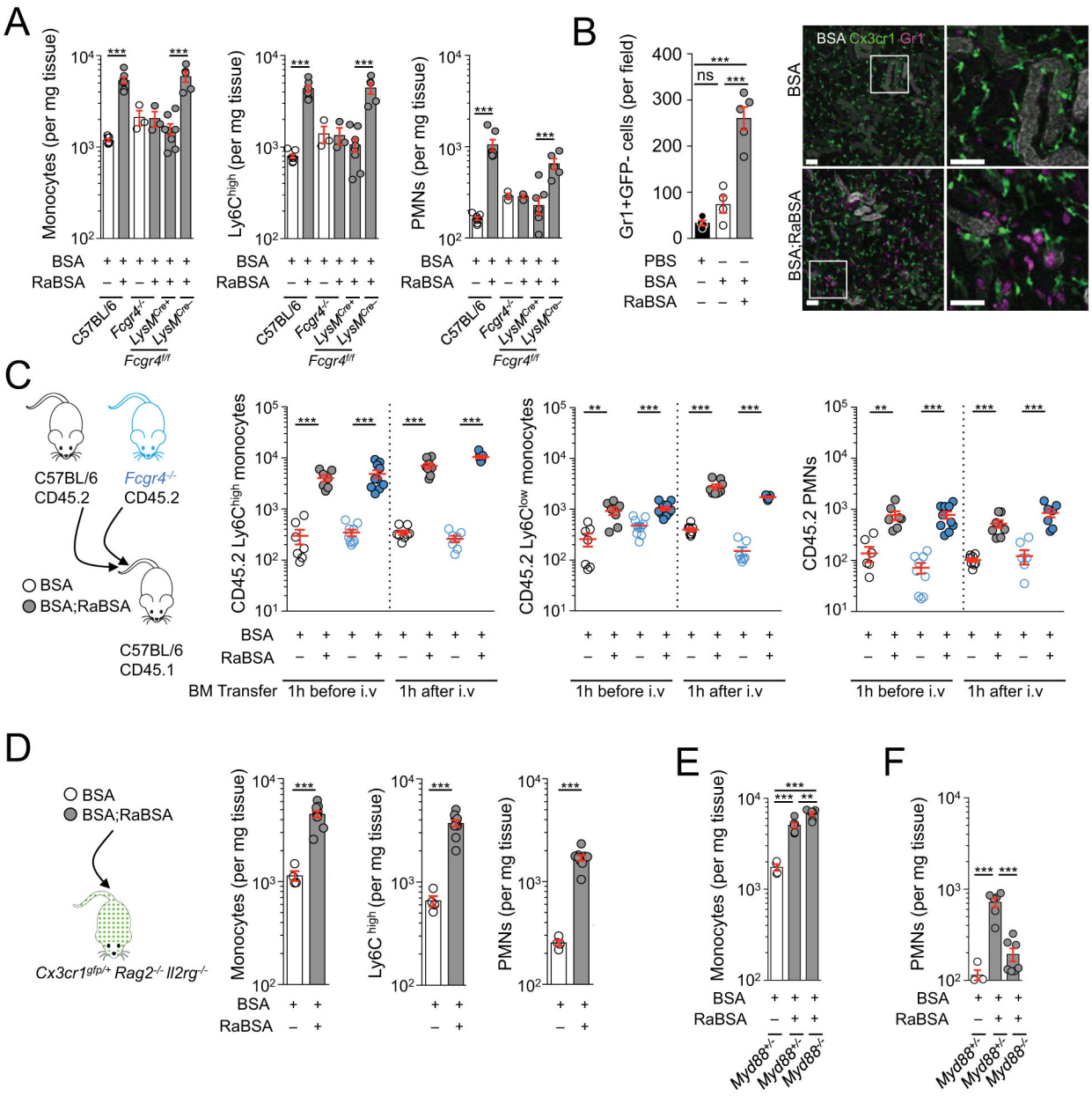

Figure 6. FcγRIV-dependent activation of kidney macrophage by immune complexes triggers recruitment of blood leucocytes

(A) Recruitment of total monocytes, Ly6C^{high} monocytes and neutrophils in the kidneys of *wt*, *Fcgr4*$^{-/-}$, *LysM*$^{Cre-}$*;Fcgr4*$^{f/f}$ and *LysM*$^{Cre+}$*;Fcgr4*$^{f/f}$ mice, assessed by flow cytometry 6 hours after *i.v.* injection of 50 μg BSA-TRITC or BSA-TRITC;RaBSA. N = 3–7 mice per treatment, per genotype. **(B)** Intravital microscopy analysis of neutrophil recruitment in the kidneys of *Cx3cr1*$^{gfp/+}$ *Rag2*$^{-/-}$ *Il2rg*$^{-/-}$ mice (detected by *i.v.* injection of APC-conjugated anti-Gr1 antibody) 6 hours after *i.v.* injection of 50 μg BSA or BSA;RaBSA. N = 4–5 mice per treatment, per genotype. Bars = 50 μm. **(C)** Recruitment of CD45.2 bone marrow leucocytes transferred from *wt* or *Fcgr4*$^{-/-}$ mice into *wt* CD45.1 recipients 1hr before or 1 hr after *i.v.* injection of 50 μg BSA-TRITC or BSA-TRITC;RaBSA. Recruitment is measured 6

hours after treatment. N = 7–10 mice per treatment, per genotype, per time point of transfer. **(D)** Recruitment of total monocytes, Ly6C^{high} monocytes and neutrophils (PMNs) in the kidneys of *Cx3cr1*$^{gfp/+}$ *Rag2*$^{-/-}$ *Il2rg*$^{-/-}$ mice 6 hours after treated as in (A). N = 4–10 mice per treatment. **(E–F)** Recruitment of total monocytes (E) and neutrophils (F) in the kidneys of *Myd88*$^{+/-}$ or *Myd88*$^{-/-}$ littermates treated as in (A). N = 4–7 mice per treatment, per genotype. Each symbol represents an individual mouse. **P < 0.01, ***P < 0.001 using a two-tailed, unpaired t-test. NS, not significant. See also Figure S6.

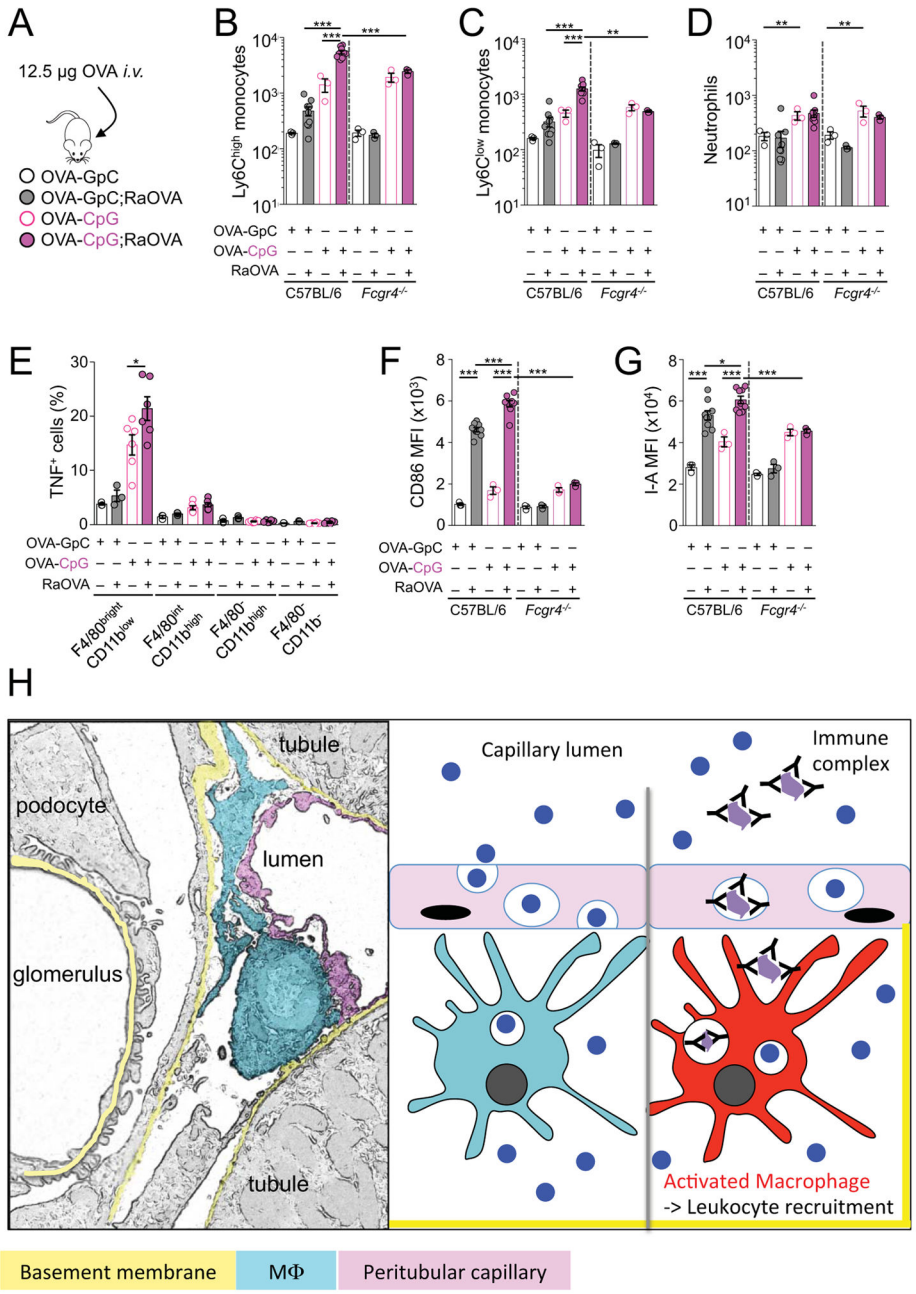

Figure 7. FcγRIV-dependent activation of macrophages by immune complexes synergizes with TLR signalling

(A) C57BL/6 or *Fcgr4*$^{-/-}$ mice were injected *i.v.* with 12.5 µg OVA-GpC, 12.5 µg OVA-CpG, OVA-GpC;RaOVA (12.5 µg OVA-GpC + 42.5 µg RaOVA) or OVA-CpG;RaOVA (12.5 µg OVA-CpG + 42.5 µg RaOVA). **(B–D)** Flow cytometric analysis of Ly6C^{high} monocyte **(B)**, Ly6C^{low} monocyte **(C)** and neutrophil **(D)** recruitment (per mg of tissue) in the kidneys of C57BL/6 or *Fcgr4*$^{-/-}$ mice assessed by flow cytometry 6 hours after treatment as in (A). **(E)** Intracellular staining for TNF in kidney leukocytes from C57BL/6 mice 1 hour after treatment as in (A). **(F–G)** Flow cytometric analysis of CD86 **(F)** and I-A **(G)** expression by F4/80^{bright} kidney macrophages 2 hours after treatment as in (A). N = 3–9 mice per

treatment, per genotype. Bars indicate mean value ± S.E.M. Symbols represent individual mice. *P < 0.05, **P < 0.01, ***P < 0.001 using a two-tailed, unpaired t-test. NS, not significant.